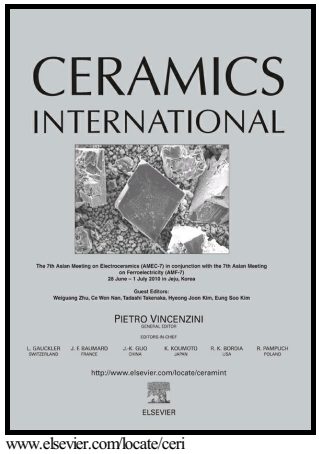

www.elsevier.com/locate/ceri

Influence of annealing temperature on structural, optical and photocatalytic properties of TiO_2-CeO_2 nanopowders

Ljiljana Rožić, Srđan Petrović, Davor Lončarević, Boško Grbić, Nenad Radić, Stevan Stojadinović, Vesna Jović, Jelena Lamovec

PII: S0272-8842(18)32811-6
DOI: https://doi.org/10.1016/j.ceramint.2018.10.153
Reference: CERI19865

To appear in: *Ceramics International*

Received date: 27 August 2018
Revised date: 2 October 2018
Accepted date: 2 October 2018

Cite this article as: Ljiljana Rožić, Srđan Petrović, Davor Lončarević, Boško Grbić, Nenad Radić, Stevan Stojadinović, Vesna Jović and Jelena Lamovec, Influence of annealing temperature on structural, optical and photocatalytic properties of TiO_2-CeO_2 nanopowders, *Ceramics International,* https://doi.org/10.1016/j.ceramint.2018.10.153

Influence of annealing temperature on structural, optical and photocatalytic properties of TiO_2-CeO_2 nanopowders

Ljiljana Rožić[1,4], Srđan Petrović[1,4*], Davor Lončarević[1], Boško Grbić[1], Nenad Radić[1], Stevan Stojadinović[2], Vesna Jović[3], Jelena Lamovec[3]

[1]*University of Belgrade, IChTM-Department of Catalysis and Chemical Engineering, Njegoševa 12, Belgrade, Republic of Serbia*

[2]*University of Belgrade, Faculty of Physics, Studentski trg 12-16, 11000 Belgrade, Republic of Serbia*

[3]*University of Belgrade, IChTM-Centre of Microelectronic Technologies, Njegoševa 12, Belgrade, Republic of Serbia*

[4]*University of Belgrade, IChTM – Centre of Excellence in Environmental Chemistry and Engineering, Njegoševa 12, Belgrade, Republic of Serbia*

[*]Corresponding author. srlepp@nanosys.ihtm.bg.ac.rs

Abstract

TiO_2-CeO_2 nanopowders were synthesised by a ball-milling process and then annealed at temperatures from 500 to 800 °C. X-ray diffraction and diffuse reflectance spectra were used in combination with temperature programmed desorption to determine the structural and microstructural changes of nanopowders as a the function of annealing temperature. The results of the X-ray analysis showed that the weight fraction of the cerianite phase remained unchanged with a temperature rise of 600 to 700 °C, indicating that the phase changes occur only within TiO_2. The TiO_2-

CeO_2 nanopowder showed enhanced optical properties with a red shift after the thermal treatment. Photocatalytic studies revealed that the sample annealed at 600 °C showed higher photocatalytic activity than samples annealed at lower or higher temperatures in the degradation of the methyl orange. The activity test of all samples is in accordance with photoluminescence measurements, proportional to the concentrations of hydroxyl radicals at the photocatalyst surfaces.

Keywords: TiO_2; CeO_2; annealing; ball milling; photocatalysis

1. Introduction

Titanium dioxide (TiO_2) and titanium oxide-based materials have shown excellent potential as powerful photocatalysts for various oxidation reactions, because of their chemical stability and high photosensitivity [1–4]. However, the large band gap (~3.2 eV) of TiO_2 makes it more active under ultraviolet (UV) light [5]. In addition, the photocatalytic activity of TiO_2 is also limited due to its high electron hole recombination rate [6]. The electron-hole recombination process is in direct competition with space-charge separation of the electron and the hole. The photocatalytic activity of TiO_2 will be increased by retarding the electron-hole recombination process [7], and a principal method of slowing electron-hole recombination is thought to be through the loading of electron accepting species on the TiO_2 surface. Accordingly, the loading of rare earth elements (Ce, Y and Eu) on TiO_2 can expedite the transport of photoexcited electrons to the outer system [8–10]. In recent years, nanocomposites of TiO_2 with cerium oxide (CeO_2) have attracted attention because of the special *f* and *d* electron orbital structures and the unique UV absorbing ability, high thermal stability and large oxygen storage capacity of CeO_2,

which remarkably improve the photocatalytic efficiency of TiO_2 [11]. In addition, in CeO_2, the oxygen defect levels are present below the conduction band, i.e., 3 eV from the valence band. Therefore, oxygen deficient ceria may have an extended absorption edge up to the visible region and have larger separation of carriers, since oxygen defects may act as electron trap centres [12].

Many techniques, such as sol-gel synthesis [13], hydrothermal synthesis [14], co-precipitation methods [15], spin coating [16], flame spray pyrolysis [17] and so on, have been employed in the formation of CeO_2-doped TiO_2. The advantages of the chemical process over the other methods for the preparation of n-type semiconducting materials are the controlled morphology, narrow particle size distribution, high purity and possible reduction in sintering temperatures. However, these methods predominantly include multi-step procedures, demanding the utilisation of toxic metal-organic precursors and expensive equipment. Therefore, among the various techniques available for the synthesis of semiconductors and photocatalysts, the mechanochemical process has certain advantages, such as low cost, the use of widely available oxides as the starting materials and skipping the calcination steps at intermediate temperatures that leads to a simplified process [18,19].

In this study, the effect of post annealing temperature is studied on structural and optical parameters. Previously, we investigated the effect of ball milling process parameters through the response surface methodology design approach on the photocatalytic efficiency of TiO_2-CeO_2 nanopowders and found that the highest photocatalytic activity was achievable at experimental conditions of TiO_2:CeO_2 weight percentage ratio 71:29, milling speed 200 rpm and milling time 115 min [20]. The structure, optical and photocatalytical properties of the TiO_2-CeO_2 nanopowders, produced by high energy ball milling and subsequent annealing at various

temperatures, were investigated using X-ray diffraction (XRD), ultraviolet-visible spectroscopy (UV-Vis) diffuse reflectance spectra (DRS) and temperature programmed desorption (TPD) of methanol. The influence of the annealing temperature on the photocatalytic activity of TiO_2-CeO_2 nanopowders in an oxidation reaction was examined.

2. Experimental

2.1. Materials

TiO_2 nanoparticles (purity >99%, particle size of ~40 μm, from Alfa Aesar GmbH & CoKG) and CeO_2 powder (99.9% purity, Johnson Matthey-Alfa Product) were used as starting materials.

2.2. Preparation of catalysts

The TiO_2-CeO_2 nanopowder was prepared by ball milling of TiO_2 powders in a high energy planetary ball mill (Fritsch planetary mill Pulverisette 7 premium line) in the presence of CeO_2 powder. Milling was done at atmospheric conditions in a silicon nitride (syalon, Si_3N_4) vial (80 cm^3) using 25 silicon nitride balls with a diameter of 10 mm, keeping the powder sample to ball mass ratio at ~1:10 throughout the experiment. The quantity of powder used in each experiment was 4.87 g, with the following weight ratio of 71% TiO_2 to 29% CeO_2. The milling process lasted for 115 min with a rotation speed of 200 rpm [20]. The obtained TiO_2-CeO_2 nanopowder was calcined for 2 h in a tube furnace at different temperatures. According to the calcination conditions, the synthesised samples were labelled as $TiCe_{500}$, $TiCe_{600}$, $TiCe_{700}$ and $TiCe_{800}$.

2.3. Characterisation of catalysts

The crystalline structure of the powders was determined by XRD (Rigaku Ultima IV X-ray diffractometer with the conventional Bragg-Brentano geometry) with Ni-filtered CuK_α radiation (40 kV, 40 mA, λ = 1.54178 Å). The crystallite sizes and microstructural parameters of the TiO_2-CeO_2 samples were estimated by Williamson-Hall plots [21]. Williamson and Hall proposed a method for the deconvolution of size and strain broadening based on the peak width as a function of 2θ. If a linear fit is obtained from the equation:

$$\beta_{hkl} = \frac{K\lambda}{D\cos\theta} + 4\varepsilon\sin\theta \quad (1)$$

it is possible to derive the crystallite size (D) from the intercept, and the micro-strain (ε) from the slope. K is a constant equal to 0.94 for spherical shaped particles, λ is the wavelength of the X-ray (1.54178 Å for CuK_α radiation) and θ is the peak centre. The weight fractions of the anatase and rutile crystalline forms of TiO_2 and the cerianite form of CeO_2 in the samples were measured by the software package Powder Cell. UV-Vis DRS of the catalysts was carried out using a UV-Vis spectrophotometer (Specord M40 Carl Zeiss). The spectra were recorded at room temperature in air within the range of 300–800 nm. The reflectance measurements were converted to absorption spectra using the Kubelka-Munk function, F(R). The absorbance F(R) can be expressed as $F(R) = (1-R)^2/2R$, where R represents the reflectance. The optical band gap value is estimated relying on the Kubelka-Munk method combined with the Tauc relation [22]:

$$(\alpha h\nu)^m = A(h\nu - E_g) \quad (2)$$

where ($h\upsilon$) is photon energy, A is a constant that depends on the properties of the material and m is constant that can take different values depending on the type of

electronic transition. By plotting $[F(R_\infty)\ h\upsilon]^m$ as a function of ($h\upsilon$), we can estimate the direct (m = 1/2) and indirect (m = 2) energy band gap (E_g). The best linear relation was obtained for m = ½, indicating that direct allowed transitions are responsible for the measured optical band gap.

TPD of methanol was performed on a Thermo Scientific 1100 TPDRO instrument coupled with a ThermoStar GSD320 mass spectrometer. Methanol was adsorbed from a 2% mixture in argon flowing at 20 mL min^{-1}. A catalyst sample of 0.17 g was exposed to the methanol containing gas at 40 °C for 1 h. Following adsorption, the reactor was purged with argon at a flow rate of 20 mL min^{-1} for at least 2 h to remove any residual methanol. For TPD experiments, the samples were heated in argon flowing at 20 mL min^{-1} at a temperature ramping rate of 5 °C min^{-1}.

A photoluminescence (PL) technique with terephthalic acid as a probe molecule was used to detect the formation of free hydroxyl radicals on the UV-illuminated TiO_2-CeO_2 surface. The experiment was conducted at ambient temperature and 0.003 g of the TiO_2-CeO_2 nanopowder annealed at different temperatures was dispersed in 10 mL of the 5×10^{-4} mol L^{-1} terephthlic acid in a diluted NaOH aqueous solution with a concentration of 2×10^{-3} mol L^{-1} in an open thermostated cell. A UV xenon lamp (450 W) was used as a light source. After UV irradiation for 3 min, the PL spectra of the reaction solution, using an excitation wavelength of 315 nm, were measured on a spectrofluorometer (Horiba Jobin Yvon Fluorolog FL3-22) at 425 nm for which the 2-hydroxyterephthalic acid exhibits an intense PL peak.

2.4. Photocatalytic activity evaluation

The photocatalytic activity of TiO_2-CeO_2 nanopowders was evaluated by performing methyl orange (MO) degradation experiments under UV irradiation. In a typical

experiment, ~100 ml of solution containing 8 mg/L MO and the 100 mg of catalysts was taken in a an open cylindrical thermostated Pyrex cell of 6.8 cm in diameter (corresponding to the surface area accessible to the light of 36.3 cm^2), and was exposed to UV light (Solimed BH Quarzlampen) for different time intervals (up to 180 min). The illumination intensity on the top of the photocatalytic reactor was 850lx. The reaction mixture solution was initially stirred for ~30 min in the dark in order to reach the adsorption equilibrium. During light irradiation, the reaction solution was continuously stirred and aliquots of the solution were taken at regular time intervals and analysed. The concentration of MO was measured by a UV-Vis spectrophotometer (Thermo Electron Nicolet Evolution 500) at a maximum absorption peak of MO at 464 nm.

The efficiency of the MO photodegradation (η) was calculated using the following equation [23]:

$$\eta = \frac{(C_0 - C)}{C_0} \times 100 \quad (3)$$

where C_0 represents the initial concentration and C represents the concentration after t minutes of photocatalysis.

3. Results and discussion

The nanopowder formed by ball milling was in the form of poorly crystalline TiO_2 anatase phase, whereas the ones formed at 500 and 600 °C were in a highly crystalline phase (Fig. 1). On further increasing the annealing temperature to 700 °C, the diffraction peaks of the anatase phase became slightly broader and its relative intensities decrease. This effect reveals the material behaviour after annealing, which should be attributed to the presence of particles with smaller sizes and the transformation of the anatase-to-rutile phase, induced by the temperature of sintering.

In addition, the powder formed at the same temperature exhibits a coexistence of anatase TiO_2 and cubic CeO_2 phases.

The results of the weight fraction of the anatase and rutile TiO_2 and cubic CeO_2 phases, as a function of temperature annealing, are presented in Fig. 2. The nanopowder formed at 500 °C contains small amounts of rutile relate to anatase. With increasing temperature from 600 to 700 °C, the rutile weight fraction increases from 24.0 to 49.6 wt.% as a consequence of the transformation of anatase to rutile. This phase transformation is related to both the changes in the relative thermodynamic stability of the nanoparticles of these two phases with particle size [24], as well as being accelerated by a temperature enhanced phase transformation rate of anatase to rutile [25,26]. After annealing at 800 °C, ~69 % of the nanopowder was transformed into the rutile phase. However, in the temperature range of 600–700 °C, the weight fraction of cerianite remained unchanged. This shows that in this temperature interval the phase changes take place only within TiO_2.

The crystallite size and lattice strain of annealed TiO_2-CeO_2 nanopowders were estimated by XRD peak broadening using the William-Hall method and the results are shown in Fig. 3. Up to 700 °C, the crystallite size increases rapidly to ~23 and 43 nm for the anatase and rutile TiO_2 phases, respectively, and after this temperature, a small decrease was registered for anatase. This is in accordance with the published data [27] showing that larger anatase microcrystals transform to rutile easier than the smaller ones.

In addition, the competing reactions between the growth of existing anatase nanocrystallites and the creation of new anatase nuclei by the crystallisation of the amorphous fractions are the main reasons for the easier growth of the anatase crystallite size during heating.

The insert of Fig. 3 shows the micro-strain curves versus annealing temperatures for anatase TiO_2 phases in TiO_2-CeO_2 nanopowders (Fig. 3). With the increase of annealing temperature in the range of 500–700 °C, the lattice microstrains decrease gradually, and values of the sample annealed at 800 °C tend to be ~0.01%. This could indicate that the strain relaxation happened during heat treatment. This is in accordance with literature data [28–30].

Alternatively, the size of cubic CeO_2 crystallites in TiO_2-CeO_2 nanopowders in the temperature range of 500–700 °C slowly decreases and increases afterwards with increasing temperature to 800 °C.

Figure 4a represents the UV-Vis diffuse reflectance spectra of pure TiO_2 samples compared with TiO_2-CeO_2 nanopowders. The raw data generating the reflectance spectra were transformed to the Kubelka-Munk function and the results are plotted in Fig. 4b. The obtained results indicated that the pure TiO_2 and the annealed at 500 °C TiO_2 powder exhibit strong photoabsorption only at wavelengths shorter than 400 nm, which occur due to the charge transfer from the valence band to the conduction band [6]. However, it can be observed that the absorption edge is shifted to longer wavelengths for annealed nanopowders. This clearly shows that the annealing process promotes changes in relation to the optical properties of the material. A possible explanation can be related to the milling and annealing process that causes the formation of particles with irregular shapes, the appearance of defects in the TiO_2 lattice and changes in its crystallite size, in agreement with the XRD results.

The specific surface, as well as the amount of acidic sites and hydroxyl radicals on the surface of the catalyst are of fundamental importance for the photocatalytic properties of the material [31]. To verify the number and nature of surface active sites, and the decomposition temperature of surface species, TPD of methanol on TiO_2-CeO_2

nanopowder was performed (Fig. 5). As can be seen in Fig. 5a, desorption of molecularly adsorbed methanol takes place at temperatures lower than 110 °C, while methoxy groups recombine at temperatures up to 250 °C or dehydrogenate to formaldehyde. Furthermore, an increase in temperature leads to the formation of dimethyl ether at 290 °C, which is formed between two adjacent methoxy groups, one adsorbed on the strong and the other on the mild Lewis acid site. At higher temperatures (340 °C), the hydrogen transfer from surface hydroxyl to a methoxy group, resulting in methane formation by C-O bond cleavage, and strongly adsorbed dehydrogenating species lead to CO formation [32]. In addition, no difference could be observed in the nature of the desorbed products after the adsorption of methanol on the TiO_2-CeO_2 nanopowder annealed at desired temperatures. In order to compare the total acidities of all samples, the areas of peaks that reflect the amounts of Lewis acid sites on the surface for all annealed samples are presented in Fig. 5b. The sample TiC_{500} gives a large desorption peak, implying that it has the highest number of acidic sites among the four TiO_2-CeO_2 samples rather than a different type of acid site. Based on the results presented in Fig 5b, the order of the peak area of samples is $TiCe_{500}$>> $TiCe_{600}$> $TiCe_{700}$ >>$TiCe_{800}$. The acidity of the $TiCe_{600}$ is similar to that of $TiCe_{700}$ and can be attributed to their similar surface properties, including surface area and surface chemistry [33]. Generally, increasing annealing temperature affects the surface acidity. In order to relate this property with photocatalytic activity, it should be considered that two reactants are taking a part in the reaction, organic pollutants and the light as an immaterial reagent. It is not expected that the surface acidity influence interaction of the light with the surface of photocatalyst but adsorption of the organic pollutants could be significantly affected. Therefore, this surface property should be considered for the efficiency of the overall photocatalytic process.

Since hydroxyl radicals are an important reaction species in the photocatalytic process [34], the formation of free hydroxyl radicals on the surface UV-illuminated TiO_2-CeO_2 nanopowder is tested and detected by the PL method with terephthalic acid as a probe molecule [35]. Figure 6 shows the change of the PL spectra of the TiO_2-CeO_2 nanopowder annealed at different temperatures. It can be seen that an obvious difference in PL intensity at ~425 nm is observed in different samples. For the $TiCe_{600}$ sample, the formation rate of hydroxyl radicals on its surface is much higher than that of other samples.

This suggests that the surface of the TiO_2-CeO_2 nanopowder inhibits the production of hydroxyl radicals when the annealing temperature is lower or higher than 600 °C, which implies that when the temperatures is 600 °C, the photocatalytic oxidation activity of $TiCe_{600}$ is much higher than any other samples.

The photocatalytic activity of TiO_2-CeO_2 nanopowders annealed at different temperatures was evaluated in terms of degradation of MO under UV light irradiation. In addition, the reduction in the concentration of the MO without visible light irradiation was very low with a degradation percent of 2.2%. This result generally shows that the system has reached the adsorption-desorption equilibrium.

The UV-Vis spectra of the photocatalytic degradation of MO over $TiCe_{500}$ sample are presented in Fig. 7. As can be observed, the maximum absorption peak, at 464 nm, gradually decreases during UV irradiation. In the presence of this sample, the colour of the dye changed from orange to light yellow, indicating that the chemical oxidation-reduction mechanisms occur on the surface of the sample. A reasonably high degradation rate of ~80% of MO within 45 min is detected over the surface of this sample.

Using the absorption spectra of all the nanopowders annealed at different temperatures, it was possible to calculate the corresponding photodegradation efficiencies by applying Eq. (3). Figure 8a shows time profiles of the photodegradation of MO over the annealed TiO_2-CeO_2 nanopowders. As can be seen, the TiCe sample shows the lowest photoactivity, although it has the highest surface acidities compared to the annealed samples. This may be related to its poor anatase crystallinity and the anatase/rutile ratio (Fig. 2), because the degree of crystallisation of anatase and the anatase/rutile ratio plays an important role in photoactivity. In addition, the values of lattice microstrain of anatase (insert of Fig. 3) indicate low crystallinity that significantly decrease after annealing. The $TiCe_{600}$ sample, with anatase crystallinity and an anatase/rutile ratio of 2:1, possesses the highest photocatalytic efficiency, about five times that of the TiCe sample. Furthermore, the $TiCe_{700}$ sample still exhibits high photocatalytic efficiency. These results clearly showed that the annealed samples could be very prominent photocatalysts.

The photodegradation of MO under UV follows first-order kinetics, as shown by the apparent first order linear transform:

$$\ln\left(\frac{C_0}{C}\right) = kt \qquad (4)$$

in Fig. 8b, where k is the apparent rate constant (h^{-1}), C_0 and C are the initial and reaction concentration of MO, respectively, and t is the time of irradiation. The relationship between $\ln(C_0/C)$ and t was fitted with linear regression lines (R^2>0.98). The calculated values for the apparent rate constants are reported in **Table 1**, showing that the highest value corresponds to $TiCe_{600}$.

In cases when the annealing temperature rises up to 800 °C, it is observed that the $TiCe_{600}$ sample has the highest rate constant in the examined time interval, about two

times higher than the rate constants for $TiCe_{500}$ and $TiCe_{700}$. The improvement in the efficiency of the MO degradation can be attributed to: a) the MO molecules being immobilised by the solid acid sites that can be attacked by the photoinduced electrons and holes on the catalyst surface via direct photooxidation mechanism [14] and b) the OH• surface group is considered to be the most active species for the oxidation of MO molecules and is generated from the oxidation of the hydroxyl radicals by the photogenerated holes [36]. These assumptions are in accordance with the concentration of hydroxyl radicals on photocatalyst surfaces (Fig. 6). Despite the lower acidity of $TiCe_{600}$ compared to $TiCe_{500}$ that is the measure of MO surface concentration, $TiCe_{600}$ has the higher activity, indicating the importance of life duration of electron/hole pair.

Conclusions

In the present study, a TiO_2-CeO_2 nanopowder was synthesised using a high energy ball-milling process under optimal conditions obtained by the response surface methodology. The relationships between structural, optical and photocatalytic properties of the TiO_2-CeO_2 nanopowders with respect to temperature of annealing are established. XRD analysis shown that the crystallite size and rutile phase content were gradually increased with temperature rise. Simultaneously microstrain of the anatase phase significantly decreases as a consequence of surface relaxation. Compared with TiO_2, the photoexcited wavelength range of the TiO_2-CeO_2 samples annealed up to 800 °C show red shifts up ~30 nm and light absorption intensities are also improved. The TiO_2-CeO_2 sample annealed at 600 °C exhibited the highest photoactivity, which is in accordance with a higher formation rate of free hydroxyl

radicals. As a general conclusion, the ball milling is an attractive preparation method for synthesis of TiO_2-CeO_2 photocatalysts requiring further thermal treatment.

Acknowledgments

This work was supported by the Ministry of Education, Science and Technological Development of the Republic of Serbia (Projects Nos. 172 015, 172 001, 172 022, 172 035, 172 026, III 45001 and TR 32 008).

References

[1] A. Fujishima, X. Zhang, D.A. Tryk, TiO_2 photocatalysis and related surface phenomena, Surf. Sci. Rep. 29 (2008) 2129 – 2139. doi:10.1016/j.surfrep.2008.10.001.

[2] G.F. Samu, Á. Veres, S.P. Tallósy, L. Janovák, I. Dékány, A. Yepez, R. Luque, C. Janáky, Photocatalytic, photoelectrochemical, and antibacterial activity of benign by design mechanochemically synthesized metal oxide nanomaterials, Catalysis Today 284 (2017) 3 – 7.

[3] J. Dostanić, D. Lončarević, Lj. Rožić, S. Petrović, D. Mijin, D.M. Jovanović, Photocatalytic degradation of azo pyridone dye: Optimization using response surface methodology, Desalin. Water Treat. 51 (2013) 2802 – 2812.

[4] M. Rani, S.J. Abbas, S.K. Tripathi, Influence of annealing temperature and organic dyes as sensitizers on sol-gel derived TiO_2 films, Mater. Sci. Eng. B-Adv. 187 (2014) 75 – 82.

[5] J. Zhou, M. Takeuchi, A.K. Ray, M. Anpo, X.S. Zhao, Enhancement of photocatalytic activity of P25 TiO_2 by vanadium ion implantation under visible light irradiation, J Colloid Interf. Sci. 311 (2007) 497 – 501.

[6] M. Pelaez, N.T. Nolan, S.C. Pillai, M.K. Seery, P. Falaras, A.G. Kontos, P.S.M. Dunlop, J. W.J. Hamilton, J.A. Byrne, K. O'Shea, M.H. Entezari, D.D. Dionysiou, A review on the visible light active titanium dioxide photocatalysts for environmental applications, Appl. Catal. B-Environ. 125 (2012) 331 – 349.

[7] S. Petrović, Lj. Rožić, Z. Vuković, B. Grbić, N. Radić, S. Stojadinović, R.Vasilić, Structural and fractal characterization of tungstophosphoric acid modified titanium dioxide photo catalyst, J Phys. Chem. Solids 103 (2017) 95 – 102.

[8] Z. Fan, F. Meng, J. Gong, H. Li, Z. Hu, D. Liu, Enhanced photocatalytic activity of hierarchical flower like CeO_2/TiO_2 heterostructures, Mater. Lett. 175 (2016) 36 – 39.

[9] W. Ruifen, W. Fuming, A. Shengli, S. Jinling, Z. Yin, Y/Eu co-doped TiO_2: synthesis and photocatalytic activities under UV-light, J Rare Earth. 33(2) (2015) 154 – 159.

[10] S. Stojadinović, N. Radić, B. Grbić, S. Maletić, P. Stefanov, A. Pačevski, R.Vasilić, Structural, photoluminescent and photocatalytic properties of TiO_2:Eu^{3+} coatings formed by plasma electrolytic oxidation, Appl. Surf. Sci. 370 (2016) 218 – 228.

[11] G. Li, D. Zhang, J.C. Yu, Thermally stable ordered mesoporous CeO_2 / TiO_2 visible light photocatalysts, Phys. Chem. Chem. Phys. 11 (2009) 3775 – 3782.

[12] S. Ameen, M. Shaheer Akhtar, H.K. Seo, H.S. Shin, Solution-processed CeO_2/TiO_2 nanocomposite as potent visible light photocatalyst for the degradation of bromophenol dye, Chem. Eng. J 247 (2014) 193 – 198. doi:10.1016/j.cej.2014.02.104.

[13] M.R. Mohammadi, D.J. Fray, Nanostructured TiO_2 - CeO_2 mixed oxides by an aqueous sol - gel process: Effect of Ce : Ti molar ratio on physical and sensing properties, Sensor Actuat. B - Chem. 150 (2010) 631 – 640.

[14] J. Tian, Y. Sang, Z. Zhao, W. Zhou, D. Wang, X. Kang, H. Liu, J. Wang, S. Chen, H. Cai, H. Huang, Enhanced Photocatalytic Performances of CeO_2 / TiO_2 Nanobelt Heterostructures, Small 22 (2013) 3864 – 3872.

[15] C. Hao, J. Li, Z. Zhang, Y. Ji, H. Zhan, F. Xiao, D. Wang, B. Liu, F. Su, Enhancement of photocatalytic properties of TiO_2 nanoparticles doped with CeO_2 and supported on SiO_2 for phenol degradation, App. Surf. Sci. 331 (2015) 17 – 26.

[16] A.A. Ismail, H. Bouzid, Synthesis of mesoporous ceria/titania thin films for self-cleaning applications, J Colloid Interf. Sci. 404 (2013) 127 – 134.

[17] C. Chaisuk, A. Wehatoranawee, S. Preampiyaeant, S. Netphat, A. Shotipruk, J. Panpranot, B. Jongsomjit, O. Mekasuwandumrong, Preparation and characterization of CeO_2/TiO_2 nanoparticles by flame spray pyrolysis, Ceram. Int. 37 (2011) 1459 – 1463.

[18] C. Xu, S. De, A.M. Balu, M. Ojeda, R. Luque, Mechanochemikal synthesis of advanced nanomaterials for catalytic applications, Chem. Commun. 15 (2015) 6698 – 6713.

[19] K. Ralps, Ch. Hardacre, S. James, Application of heterogeneous catalysts prepared by mechanochemical synthesis, Chem. Soc. Rev. 42 (2013) 7701 – 7718.

[20] S. Petrović, Lj. Rožić, Vesna Jović, S. Stojadinović, B. Grbić, N. Radić, J. Lamovec, R. Vasilić, Optimization of a nanoparticle ball milling process parameters using the response surface method, Adv. Powder Technol. 29 (2018) 2129 – 2139. https://doi.org/10.1016/j.apt.2018.05.021

[21] V. Mote, Y. Purushotham, B. Dole, Williamson-Hall analysis in estimation of

lattice strain in nanometer-sized ZnO particles, J. Theor. Appl. Phys. 6 (2012) 6. doi:10.1186/2251 – 7235 – 6 – 6.

[22] J. Tauc, R. Grigorovici, A. Vancu, Optical properties and electronic structure of amorphous germanium, Phys. Status Solid 15 (1966) 627 – 637.

[23] R.A. Carcel, L. Andronic, A. Duta, Photocatalytic activity and stability of TiO_2 and WO_3 thin films, Mater. Charact. 70 (2012) 68 – 73. doi:10.1016/j.matchar.2012.04.021.

[24] F.Galindo - Hernández, R. Gómez, Degradation of the herbicide 2,4-dichlorophenoxyacetic acid over TiO_2 - CeO_2 sol-gel photocatalysts: Effect of the annealing temperature on the photoactivity, J. Photoch. Photobio. A 217 (2011) 383 – 388.

[25] N. Abbas, G.N. Shao, M.S. Haider, S.M. Imran, S.S. Park, H.T. Kim, Sol-gel synthesis of TiO_2-Fe_2O_3 systems: Effects of Fe_2O_3 content and their photocatalytic properties, J. Ind. Eng. Chem. 39 (2016) 112 – 120.

[26] M. Hirano, C. Nakahara, K. Ota, O. Tanaike, M. Inagaki, Photoactivity and phase stability of ZrO_2 doped anatase-- type TiO_2 directly formed as nanometer sized particles by hydrolysis under hydrothermal conditions, J. Solid State Chem. 170 (2003) 39 – 47.

[27] S. Bakardjieva, J. Šubrt, V. Štengla, M.J. Dianez, M. J. Sayagues, Photoactivity of anatase-rutile TiO_2 nanocrystalline mixtures obtained by heat treatment of homogeneously precipitated anatase, Appl. Catal. B- Environ. 58 (2005) 193 – 202.

[28] F.X. Zhao, X.C. Xu, H.Q. Liu, Y.L. Wang, Effect of annealing treatment on the microstructure and mechanical properties of ultrafine-grained aluminium, Mater. Design 53 (2014) 262 – 268.

[29] C. Wang, Y. Hou, H. Ge, M. Zhu, H. Yan, Crystal structure and orthorhombic–tetragonal phase transition of nanoscale (Li0.06Na0.47K0.47)NbO3, J. Eur. Ceram. Soc. 29 (2009) 2589 – 2594.

[30] G. H. Tariq, D. W. Lane, M. Anis-ur-Rehman, Physical properties of chalcogenide Sn–Bi–S graded thin films annealed in argon, Appl. Phys. A (2015) 120:1407 – 1414.

[31] N.P. de Moraes, F.N. Silva, M.L.C.P. da Silva, T.M.B. Campos, G.P. Thim, L.A. Rodrigues, Methylene blue photodegradation employing hexagonal prismshaped niobium oxide as heterogeneous catalyst: Effect of catalyst dosage, dye concentration, and radiation source, Mater. Chem. Phys. 214 (2018) 95 – 106.

[32] J.M. Tatibouët, Methanol oxidation as a catalytic surface probe, Appl. Catal. A-Gen. 148 (1997) 213 – 252.

[33] M.R. Hoffmann, S.T. Martin, W. Choi, D.W. Bahnemannt, Environmental applications of semiconductor photocatalysis, Chem. Rev. 95 (1995) 69 – 96.

[34] I.H. Chowdhury, S. Kundu, M.K. Naskar, Effect of organic acids on the phisikochemical properties of titania and its photodegradation efficiency of methyl orange, J Phys. Chem. Solids 121 (2018) 367 – 374.

[35] W. Liu, M. Ji, S. Chen, Preparation, characterization and activity evaluation of $Ag_2Mo_4O_{13}$ photocatalyst, J. Hazard. Mater. 186 (2011) 2001 – 2008.

[36] Z. Dohcevic-Mitrovic, S. Stojadinović, L. Lozzi, S. Aškrabić, M. Rosić, N. Tomić, N. Paunović, S. Lazović, M.G. Nikolić, S. Santucci, WO_3/TiO_2 composite coatings: Structural, optical and photocatalytic properties, Mater. Res. Bull. 83 (2016) 217 – 224. doi:10.1016/j.materresbull.2016.06.011.

Fig 1. XRD patterns of the TiO_2-CeO_2 nanopowders annealed at different temperatures (from 500 to 800 °C). **A** – anatase; **R** – rutile; **C** - cerianite

Fig 2. The weight fraction of anatase and rutile TiO_2 phases and cubic CeO_2 phase in TiO_2-CeO_2 nanopowders annealed at different temperatures.

Fig 3. Comparison of the average crystallite size and strain in TiO_2-CeO_2 samples as a function of annealing temperatures. Insert: variation of the microstrain in anatase phase of TiO_2 with the annealing temperature.

Fig 4. (a) Uv-Vis diffuse reflectance spectra of pure TiO_2 samples compared with TiO_2-CeO_2 samples annealed at temperatures from 500 to 800 °C. (b) The plot of transformed Kulbeka-Munk function versus hυ.

Fig 5. Methanol TPD profiles of TiO_2-CeO_2 samples annealed: (a) at 500 °C and (b) from 500 to 800 °C.

Fig 6. PL spectral changes observed during UV illumination of pure terephthalic acid and TiO_2-CeO_2 samples (annealed at temperatures from 500 to 800 °C) in the solution of terephthalic acid after 3 min.

Fig 7. UV-Vis spectra of the photocatalytic degradation of MO on the $TiCe_{500}$ sample.

Fig 8. Photocatalytic degradation over time, of MO aqueous solution in the presence of TiO_2-CeO_2 photocatalysts. The insert shows the plot of $\ln(C_0/C)$ versus time.

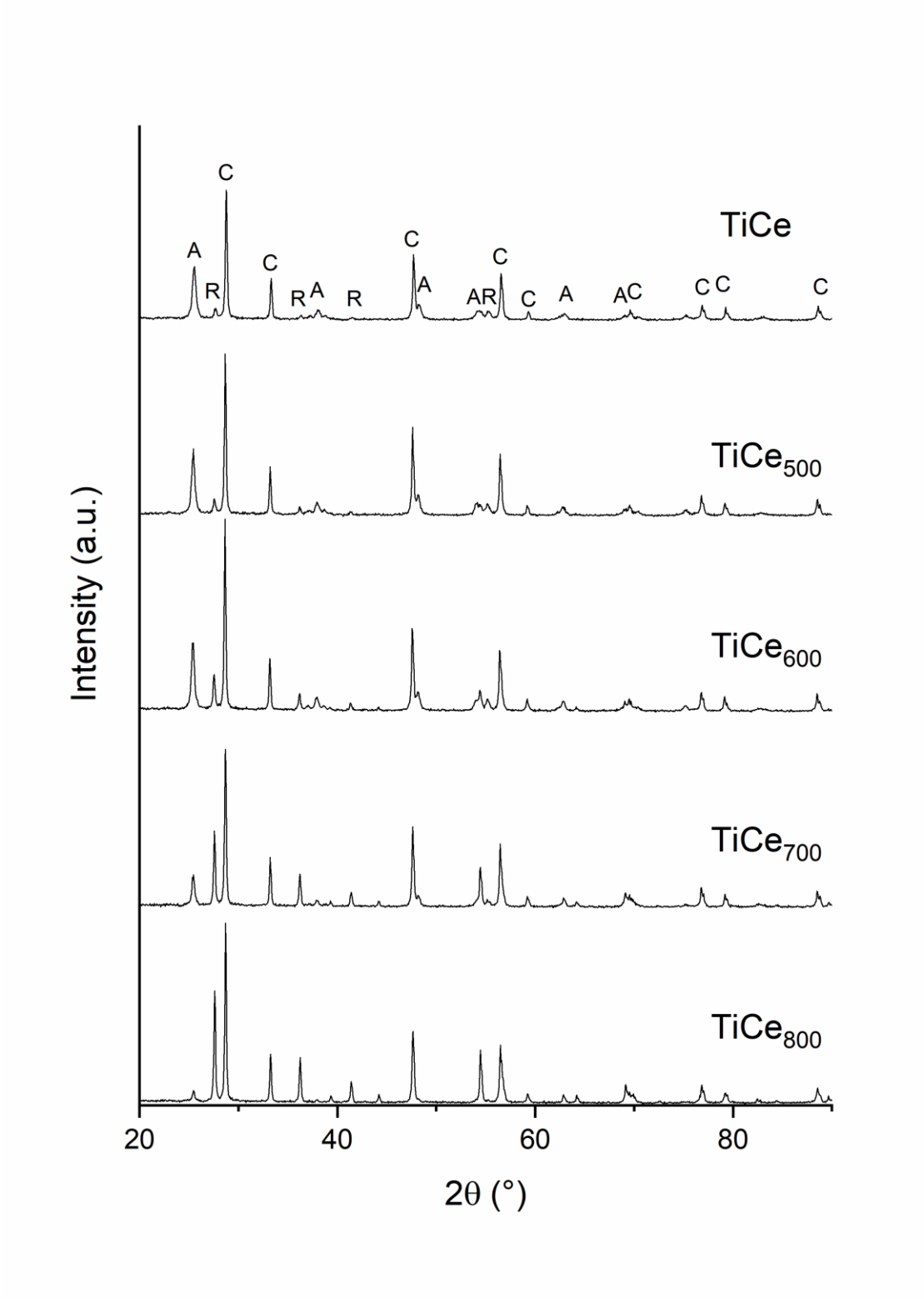
TiCe
TiCe500
TiCe600
TiCe700
TiCe800
Intensity (a.u.)
2θ (°)
20
40
60
80
A
R
C

Fig. 1

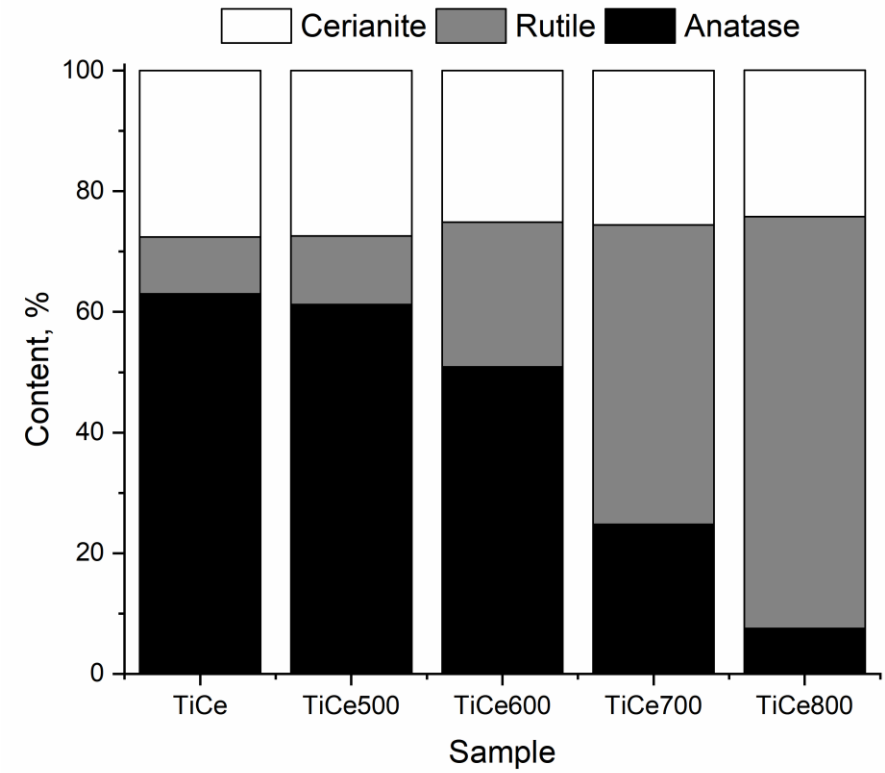
Cerianite
Rutile
Anatase
Content, %
100
80
60
40
20
0
TiCe
TiCe500
TiCe600
TiCe700
TiCe800
Sample

Fig. 2

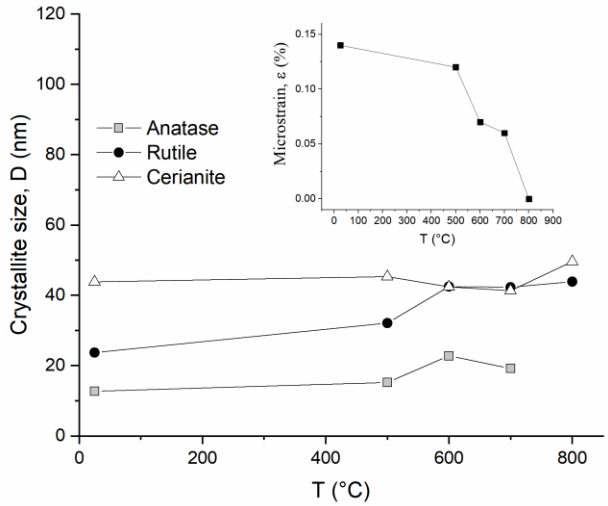
Crystallite size, D (nm)
Anatase
Rutile
Cerianite
T (°C)
Microstrain, ε (%)
0.15
0.10
0.05
0.00
0 100 200 300 400 500 600 700 800 900
T (°C)

Fig. 3

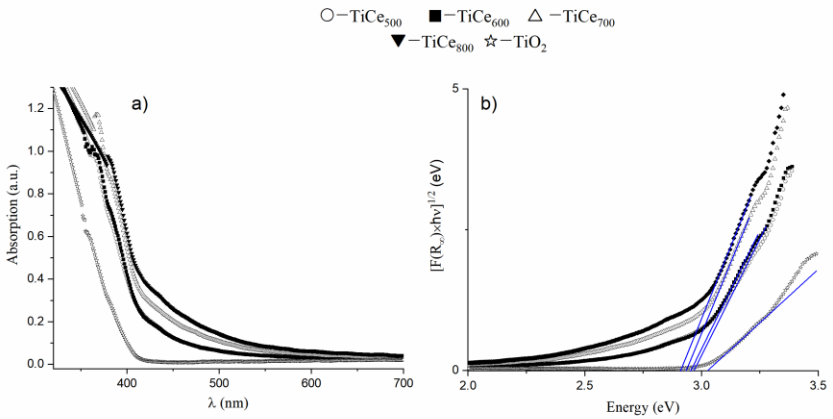
○−TiCe500 ■−TiCe600 △ −TiCe700
▼−TiCe800 ☆−TiO2
a)
Absorption (a.u.)
λ (nm)
b)
[F(R∞)×hν]1/2 (eV)
Energy (eV)

Fig. 4

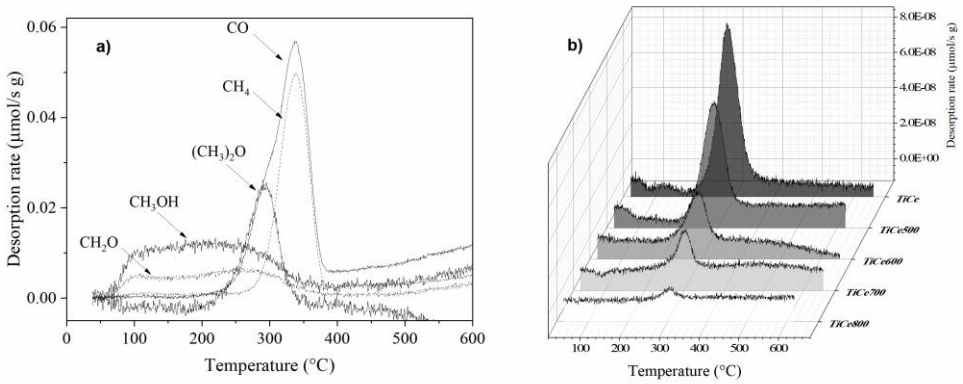
a)
CO
CH4
(CH3)2O
CH3OH
CH2O
Desorption rate (μmol/s g)
Temperature (°C)
b)
TiCe
TiCe500
TiCe600
TiCe700
TiCe800
Desorption rate (μmol/s g)
Temperature (°C)

Fig. 5

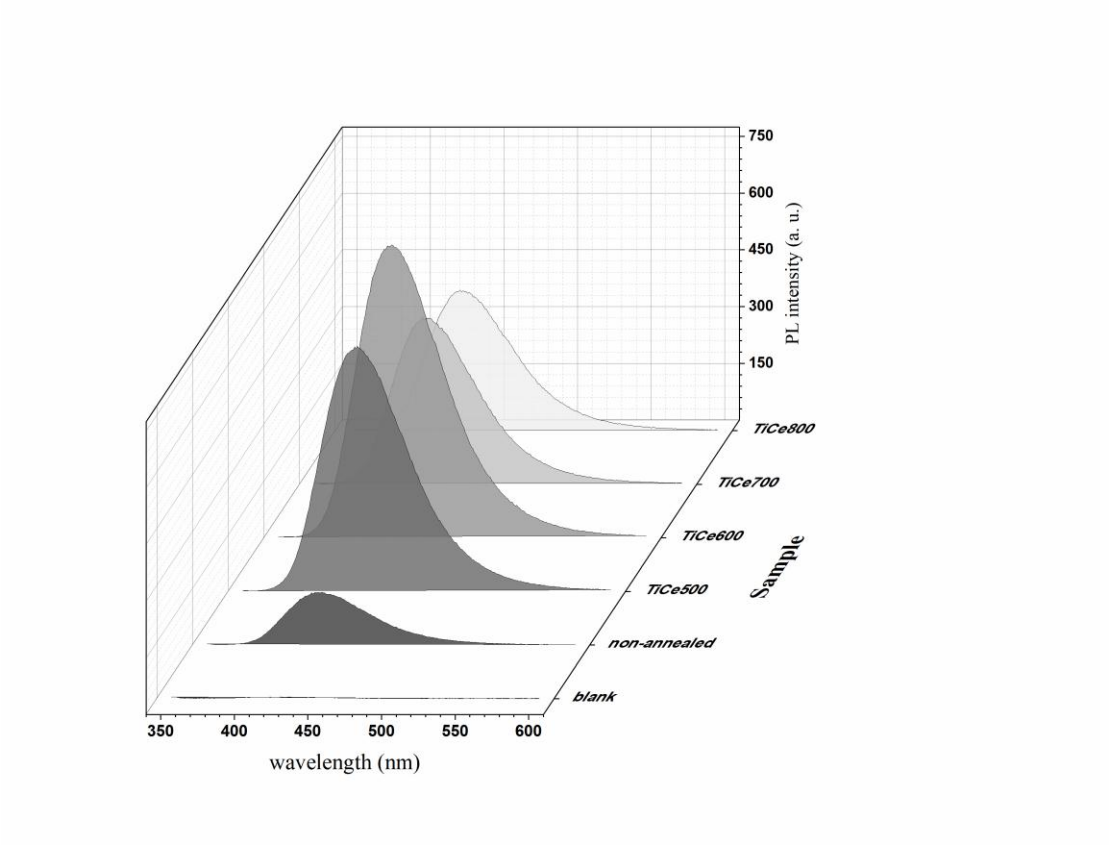

Fig. 6

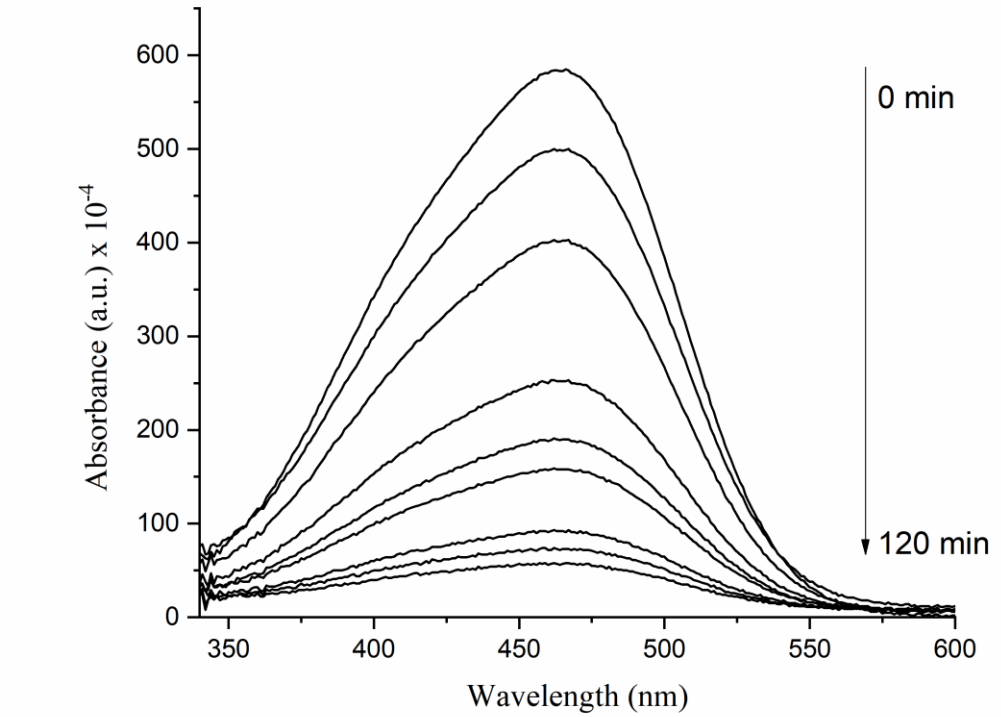
Absorbance (a.u.) x 10^{-4}
Wavelength (nm)
0 min
120 min
0
100
200
300
400
500
600
350
400
450
500
550
600

Fig. 7

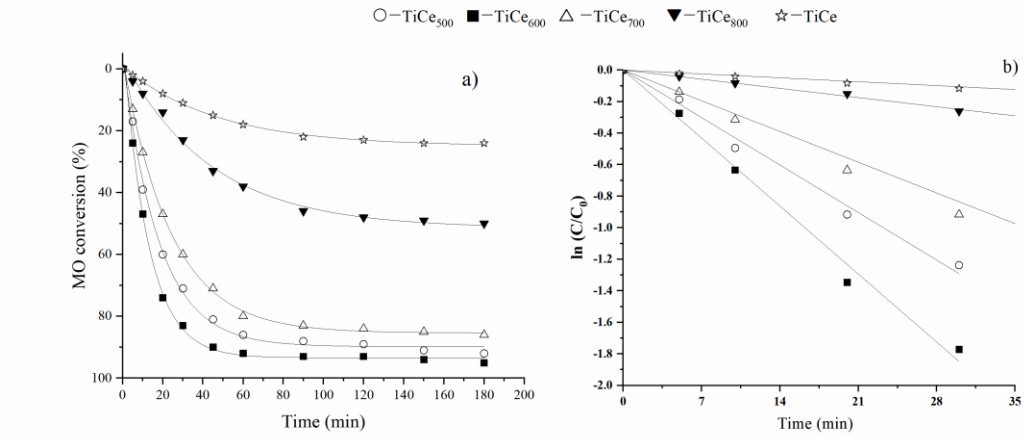
$TiCe_{500}$ $TiCe_{600}$ $TiCe_{700}$ $TiCe_{800}$ TiCe
a)
MO conversion (%)
Time (min)
b)
ln (C/C_0)
Time (min)

Fig. 8

Table 1. Apparent first-order kinetics equations and relative parameters for photodegradation of MO with TiO_2-CeO_2 photocatalysts

Sample	Kinetics equation	k (h^{-1})	R^2
TiCe	$\ln(C_0/C) = 0.0042\ t - 0.0011$	0.253	0.999
$TiCe_{500}$	$\ln(C_0/C) = 0.0477\ t - 0.0247$	2.864	0.979
$TiCe_{600}$	$\ln(C_0/C) = 0.0715\ t - 0.0817$	4.288	0.999
$TiCe_{700}$	$\ln(C_0/C) = 0.0329\ t - 0.0208$	1.973	0.998
$TiCe_{800}$	$\ln(C_0/C) = 0.0073\ t - 0.0071$	0.435	0.992